

Supplement of Atmos. Chem. Phys., 18, 17615–17635, 2018
<https://doi.org/10.5194/acp-18-17615-2018-supplement>
© Author(s) 2018. This work is distributed under
the Creative Commons Attribution 4.0 License.



Supplement of

Marine boundary layer aerosol in the eastern North Atlantic: seasonal variations and key controlling processes

Guangjie Zheng et al.

Correspondence to: J. Wang (jian@wustl.edu)

The copyright of individual parts of the supplement might differ from the CC BY 4.0 License.

S1. Data filtering methods

The Graciosa Airport is located nearby the ENA site, with the east-west extending aircraft runway 116 m north of the site (Wood et al., 2015). Pollution episodes associated with aircraft and road vehicles at Graciosa Airport are identified and screened out based on temporal variation of CN, following a similar method as described in Zheng et al. (2016). Briefly, the change rate of total aerosol number concentration (CN) is calculated first. Subsequently, all time points with change rates larger than $60 \text{ cm}^{-3} \text{ s}^{-1}$, which is roughly the 95th percentile of all CN change rates, are identified as episode candidates. Starting from these candidates, the program will look forward / backward until all pollution periods is found (Zheng et al., 2016). This method worked satisfactorily as a conservative estimate that can remove the most obvious local pollution periods, which typically constitutes 0 %~20 % of the data within the averaging interval of 1-h.

10

With this filter, data impacted by local ship emissions are also screened out. Langley et al. (2010) shows that ship particle emissions, when present, can contribute substantially to particle and CCN concentration in the MBL. That condition, if present in ENA, would also be screened out considering the high aerosol number concentration ($1000 \sim 3500 \text{ cm}^{-3}$). The contribution of the ship particle emissions averaged over large spatial area in remote marine boundary layer remains unclear, therefore it is not directly treated in this study.

15

S2. Optical data corrections

B_{abs} can be derived by Bond's correction of: $B_{\text{abs}} = B_{\text{PSAP}} - 0.0164 B_{\text{NEPH}}$ (Bond et al., 1999). For this purpose, conversion of B_{NEPH} from Nephelometer measurement wavelengths (450, 550, and 700 nm) to 3λ -PSAP measurement wavelengths (464, 529, and 648 nm) is needed, through interpolation based on the Scattering Ångström Exponent (SAE) (Costabile et al., 2013). For example, B_{NEPH} at 529 nm are derived by:

20

$$SAE_{\text{NEPH}}(550) = -\frac{\log(B_{\text{NEPH}}(700)/B_{\text{NEPH}}(450))}{\log(700/450)}, \text{ and } B_{\text{NEPH}}(529) = B_{\text{NEPH}}(550) \left[\left(\frac{529}{550} \right)^{-SAE_{\text{NEPH}}(550)} \right]$$

where the numbers in parenthesis denoted the wavelengths in nm. Similarly, B_{NEPH} at 464 and 648 nm were derived from those measured at from 450 and 700 nm, using SAE derived by 450 nm /550 nm and 550 nm /700 nm wavelength pairs. Note that there's another correction method proposed by Virkkula et al. (Bond et al., 1999; Virkkula et al., 2005; Virkkula, 2010). Based on our data, that correction will result in a 6 % lower value in B_{abs} at 529 nm, but showing the same trend with Bond' correction ($R^2=0.99$). As here we only discussed about relative trends in B_{abs} here, the detailed correction method would not influence our conclusions.

25

For B_{sca} , truncation and angular illumination corrections using SAE are applied, following the method proposed by Anderson and Ogren (1998). Briefly, that is $B_{\text{sca}} = (a+b \cdot SAE) \cdot B_{\text{NEPH}}$, where the wavelength-dependent correction coefficient $a(\lambda)$ and $b(\lambda)$ are taken from Müller et al. (2011), with the “sub- μm ” and “no cut” coefficients applied for PM_{10} and PM_{10} signals, respectively. After this correction, B_{sca} is further converted to PSAP-corresponding wavelengths through the SAE interpolation method as described above. Again, take data at 529 nm for example, it was derived by:

30

$$SAE(550) = -\frac{\log(B_{\text{sca}}(700)/B_{\text{sca}}(450))}{\log(700/450)}, \text{ and } B_{\text{sca}}(529) = B_{\text{sca}}(550) \left[\left(\frac{529}{550} \right)^{-SAE(550)} \right]$$

S3. Estimation of k_{CCN} and k_{CN}

For $CCN(0.1\%)_{SSA}$, the influence of secondary processing is expected to be negligible. SSA over 100 nm would all have been activated under typical cloud ss , thus the ratio of $CCN(0.1\%)_{SSA}$ to N_{400} would be conserved during coalescence scavenging. Non-cloud processing would reduce N_{Ac} through coagulation loss, while this influence is expected to be small (section 6.2, Table 3). Thus we have $k_{CCN} = 1$.

In terms of CN , the situation could be more complicated since it includes both CCN and interstitial aerosols. Coalescence scavenging would reduce $CCN(0.1\%)_{SSA}$ without impacting the interstitial aerosols, thus elevating actual $CN/CCN(0.1\%)_{SSA}$ ratio and underestimating the CN_{SSA} . To the contrary, coagulation loss and interstitial scavenging could be a major non- CCN loss term (section 6.2, Table 3), which will result in a lower actual $CN/CCN(0.1\%)_{SSA}$ ratio than theoretically predicted, and thus an overestimation in estimated CN_{SSA} . The overall influence depends on the relative strength of these two mechanisms. Assuming that both the $CCN(0.1\%)_{SSA}$ and the interstitial aerosols from SSA, $N_{INT,SSA}$, are in steady state (namely $\partial_t CCN(0.1\%)_{SSA} = 0$ and $\partial_t N_{INT,SSA} = 0$), then we have:

$$\begin{aligned} \int_{\ln 100}^{\ln 1000} f_{SSA}(\ln D_p) d \ln D_p &= (E_{CCN|PRCP} + E_{CCN|COND} + E_{CCN|FT,dilute}) CCN(0.1\%)_{SSA} \\ \int_{\ln 10}^{\ln 100} f_{SSA}(\ln D_p) d \ln D_p &= (E_{CN-CCN|INT} + E_{CN-CCN|COAG} + E_{CN-CCN|COND} + E_{FT,dilute}) N_{INT,SSA} \\ &= (E_{CN-CCN|INT} + E_{CN-CCN|COAG} + E_{CN-CCN|COND} + E_{FT,dilute}) (CN_{SSA} - CCN(0.1\%)_{SSA}) \end{aligned}$$

where $E_{FT,dilute}$ is the dilution efficiency of FT air being $-\omega_s/H_{MBL}$ (section 5). Combing these two equations, we have:

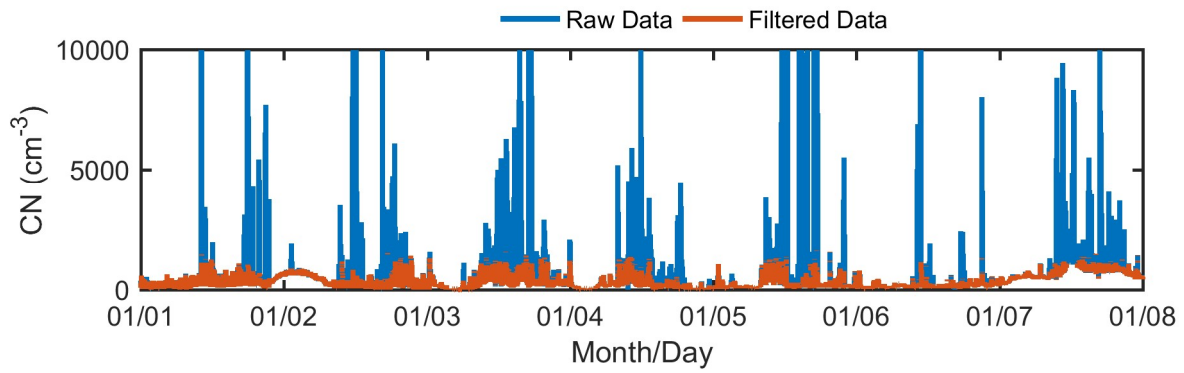
$$\begin{aligned} \frac{CN_{SSA} - CCN(0.1\%)_{SSA}}{CCN(0.1\%)_{SSA}} &= \frac{E_{CCN|COALES} + E_{CCN|COND} + E_{FT,dilute}}{E_{CN-CCN|INT} + E_{CN-CCN|COAG} + E_{CN-CCN|COND} + E_{FT,dilute}} \frac{\int_{\ln 10}^{\ln 100} f_{SSA}(\ln D_p) d \ln D_p}{\int_{\ln 100}^{\ln 1000} f_{SSA}(\ln D_p) d \ln D_p} \end{aligned}$$

Thus k_{INT} could be estimated by:

$$k_{INT} = \frac{E_{CCN|COALES} + E_{CCN|COND} + E_{FT,dilute}}{E_{CN-CCN|INT} + E_{CN-CCN|COAG} + E_{CN-CCN|COND} + E_{FT,dilute}} < \frac{E_{CCN|COALES}}{E_{CN-CCN|INT} + E_{CN-CCN|COAG}}$$

The estimated coalescence scavenging efficiency (17% ~ 40% CCN day⁻¹) is 1.7-4.4 times stronger than the overall efficiency of coagulation loss and interstitial scavenging (Table 3). Correspondingly, the upper limit of k_{INT} is expected to be between 1.7 and 4.4 (Table 4).

Fig. S1 to S6



5 **Figure S1. Raw and filtered CN during the first week in Jan. 2017, as an example of the outcome of the pollution episode filtering method used here.**

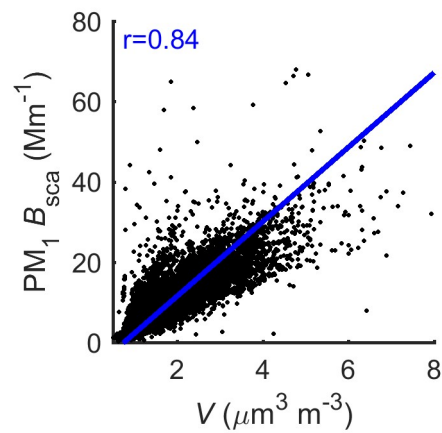


Figure S2. Correlation of PM₁ B_{sca} and total volume concentration derived from UHSAS measurements from 2015 to 2017. The value of r given referred to the Pearson correlation coefficient, while the regression line based on York et al. (2004) is also shown for reference.

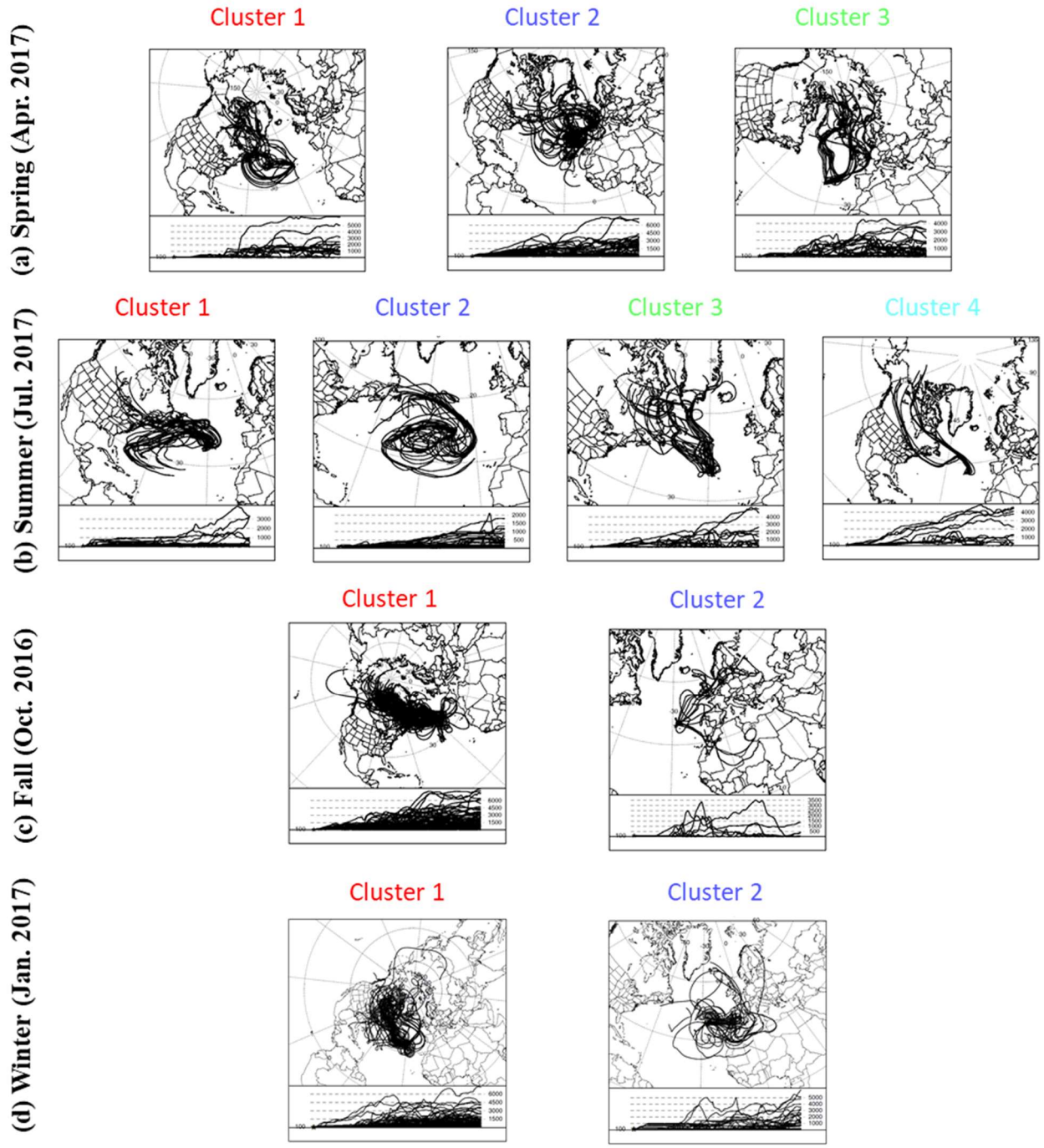


Figure S3. Detailed trajectories for each cluster shown in Fig. 1.

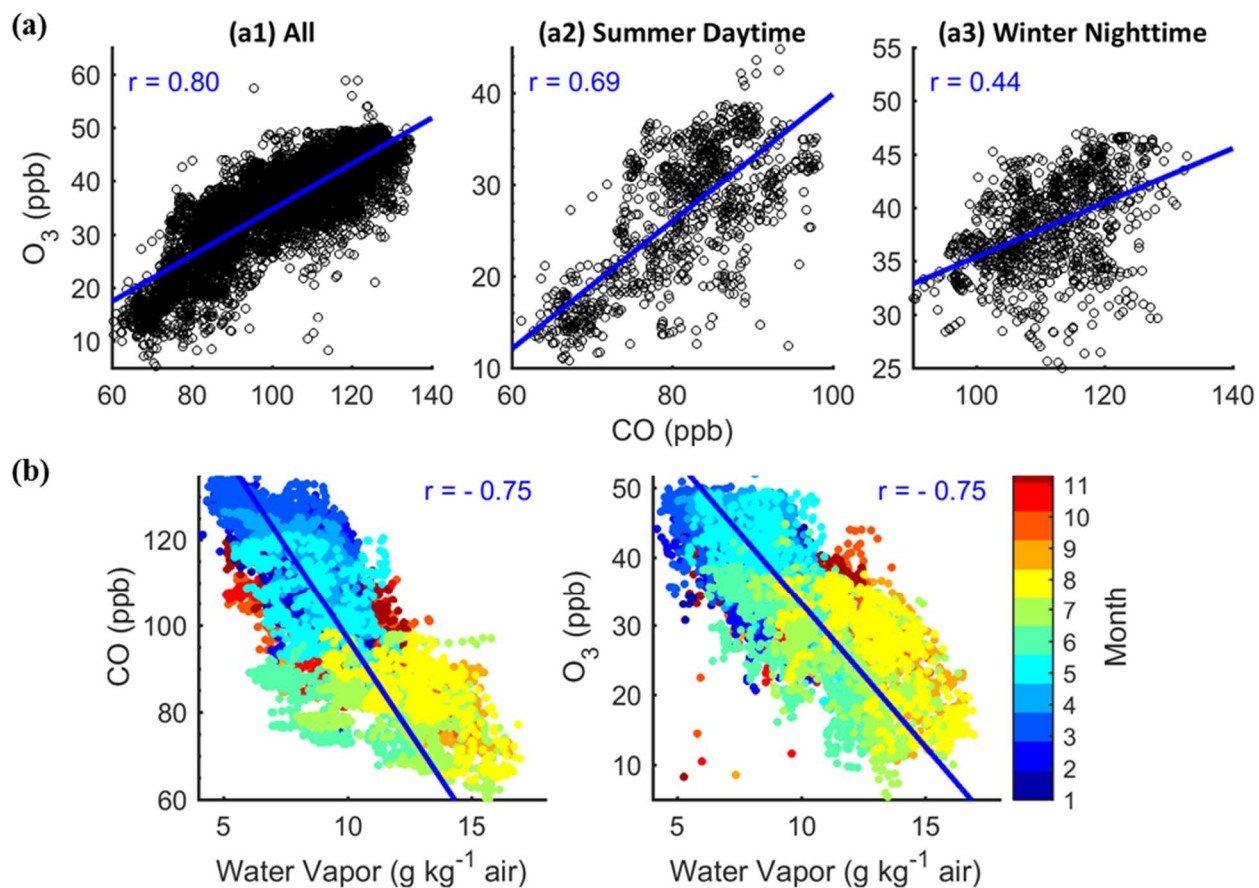


Figure S4. Evidences of FT domination on ENA CO and O₃. (a) O₃-CO correlations during (a1) all periods, (a2) summer daytime and (a3) winter nighttime, where daytime indicated 8:00 to 20:00 LT. (b) Correlation of CO and O₃ with water vapor. Data during the identified dust and biomass burning episodes (section 3.3) is excluded here. The value of r given referred to the Pearson correlation coefficient, while the regression line based on York et al. (2004) is also shown for reference.

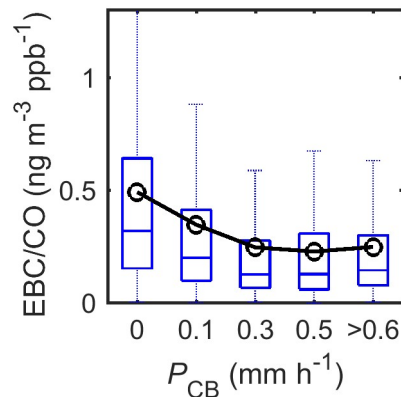
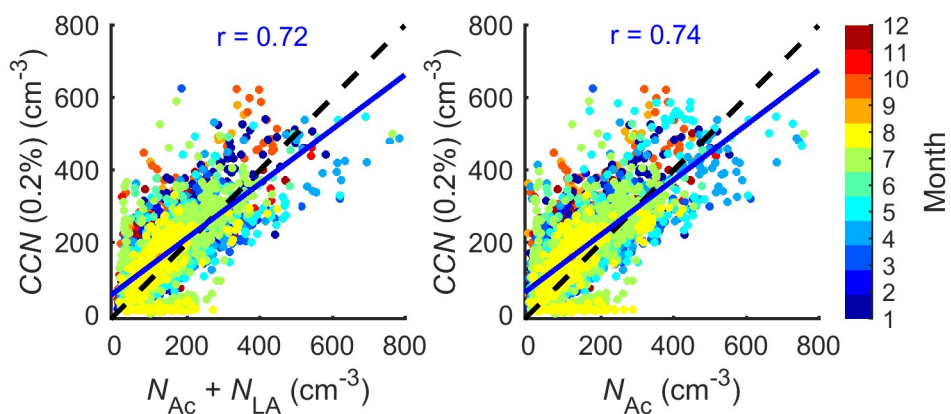


Figure S5. Dependence of EBC to CO ratio with precipitation rate at cloud base (P_{CB}).



5 **Figure S6. Comparison of observed CCN concentrations with relevant modal number concentrations.** The black dash line is the 1:1 line shown for reference. The value of r given referred to the Pearson correlation coefficient, while the regression line based on York et al. (2004) is also shown for reference.

References

- Anderson, T. L., and Ogren, J. A.: Determining Aerosol Radiative Properties Using the TSI 3563 Integrating Nephelometer, *Aerosol Science and Technology*, 29, 57-69, 10.1080/02786829808965551, 1998.
- Bond, T. C., Anderson, T. L., and Campbell, D.: Calibration and Intercomparison of Filter-Based Measurements of Visible Light
5 Absorption by Aerosols, *Aerosol Science and Technology*, 30, 582-600, 10.1080/027868299304435, 1999.
- Costabile, F., Barnaba, F., Angelini, F., and Gobbi, G. P.: Identification of key aerosol populations through their size and composition resolved spectral scattering and absorption, *Atmos. Chem. Phys.*, 13, 2455-2470, 10.5194/acp-13-2455-2013, 2013.
- Langley, L., Leaitch, W. R., Lohmann, U., Shantz, N. C., and Worsnop, D. R.: Contributions from DMS and ship emissions to CCN observed over the summertime North Pacific, *Atmos. Chem. Phys.*, 10, 1287-1314, 10.5194/acp-10-1287-2010, 2010.
- 10 Müller, T., Laborde, M., Kassell, G., and Wiedensohler, A.: Design and performance of a three-wavelength LED-based total scatter and backscatter integrating nephelometer, *Atmos. Meas. Tech.*, 4, 1291-1303, 10.5194/amt-4-1291-2011, 2011.
- Virkkula, A., Ahlquist, N. C., Covert, D. S., Arnott, W. P., Sheridan, P. J., Quinn, P. K., and Coffman, D. J.: Modification, Calibration and a Field Test of an Instrument for Measuring Light Absorption by Particles, *Aerosol Science and Technology*, 39, 68-83, 10.1080/027868290901963, 2005.
- 15 Virkkula, A.: Correction of the Calibration of the 3-wavelength Particle Soot Absorption Photometer (3 λ PSAP), *Aerosol Science and Technology*, 44, 706-712, 10.1080/02786826.2010.482110, 2010.
- Wood, R., Wyant, M., Bretherton, C. S., Rémillard, J., Kollias, P., Fletcher, J., Stemmler, J., Szoeke, S. d., Yuter, S., Miller, M., Mechem, D., Tselioudis, G., Chiu, J. C., Mann, J. A. L., O'Connor, E. J., Hogan, R. J., Dong, X., Miller, M., Ghate, V., Jefferson, A., Min, Q., Minnis, P., Palikonda, R., Albrecht, B., Luke, E., Hannay, C., and Lin, Y.: Clouds, Aerosols, and Precipitation in the
20 Marine Boundary Layer: An Arm Mobile Facility Deployment, *Bulletin of the American Meteorological Society*, 96, 419-440, 10.1175/bams-d-13-00180.1, 2015.
- York, D., Evensen, N. M., Martinez, M. L., and De Basabe Delgado, J.: Unified equations for the slope, intercept, and standard errors of the best straight line, *American Journal of Physics*, 72, 367-375, 2004.
- Zheng, G., Duan, F., Ma, Y., Zhang, Q., Huang, T., Kimoto, T., Cheng, Y., Su, H., and He, K.: Episode-Based Evolution Pattern
25 Analysis of Haze Pollution: Method Development and Results from Beijing, China, *Environmental Science & Technology*, 50, 4632-4641, 10.1021/acs.est.5b05593, 2016.